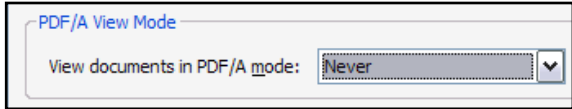
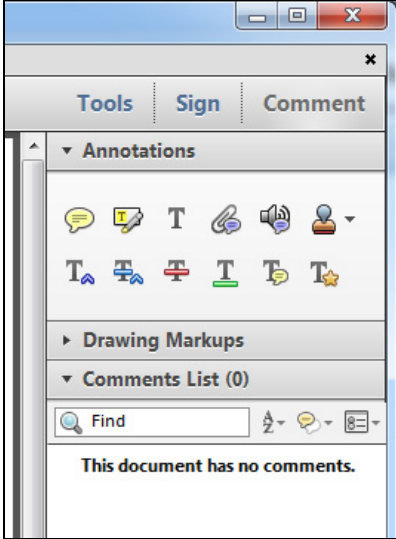


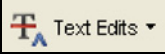
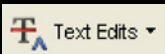
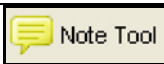
INSTRUCTIONS ON THE ANNOTATION OF PDF FILES

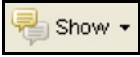
To view, print and annotate your article you will need Adobe Reader version 9 (or higher). This program is freely available for a whole series of platforms that include PC, Mac, and UNIX and can be downloaded from <http://get.adobe.com/reader/>. The exact system requirements are given at the Adobe site: <http://www.adobe.com/products/reader/tech-specs.html>.

Note: if you opt to annotate the file with software other than Adobe Reader then please also highlight the appropriate place in the PDF file.

PDF ANNOTATIONS	
Adobe Reader version 9	Adobe Reader version X and XI
<p>When you open the PDF file using Adobe Reader, the Commenting tool bar should be displayed automatically; if not, click on 'Tools', select 'Comment & Markup', then click on 'Show Comment & Markup tool bar' (or 'Show Commenting bar' on the Mac). If these options are not available in your Adobe Reader menus then it is possible that your Adobe Acrobat version is lower than 9 or the PDF has not been prepared properly.</p>  <p>(Mac)</p> <p>PDF ANNOTATIONS (Adobe Reader version 9)</p> <p>The default for the Commenting tool bar is set to 'off' in version 9. To change this setting select 'Edit Preferences', then 'Documents' (at left under 'Categories'), then select the option 'Never' for 'PDF/A View Mode'.</p>  <p>(Changing the default setting, Adobe version 9)</p>	<p>To make annotations in the PDF file, open the PDF file using Adobe Reader XI, click on 'Comment'.</p> <p>If this option is not available in your Adobe Reader menus then it is possible that your Adobe Acrobat version is lower than XI or the PDF has not been prepared properly.</p>  <p>This opens a task pane and, below that, a list of all Comments in the text. These comments initially show all the changes made by our copyeditor to your file.</p> 

HOW TO...

Action	Adobe Reader version 9	Adobe Reader version X and XI
Insert text	Click the 'Text Edits' button  on the Commenting tool bar. Click to set the cursor location in the text and simply start typing. The text will appear in a commenting box. You may also cut-and-paste text from another file into the commenting box. Close the box by clicking on 'x' in the top right-hand corner.	Click the 'Insert Text' icon  on the Comment tool bar. Click to set the cursor location in the text and simply start typing. The text will appear in a commenting box. You may also cut-and-paste text from another file into the commenting box. Close the box by clicking on 'x'  in the top right-hand corner.
Replace text	Click the 'Text Edits' button  on the Commenting tool bar. To highlight the text to be replaced, click and drag the cursor over the text. Then simply type in the replacement text. The replacement text will appear in a commenting box. You may also cut-and-paste text from another file into this box. To replace formatted text (an equation for example) please Attach a file (see below).	Click the 'Replace (Ins)' icon  on the Comment tool bar. To highlight the text to be replaced, click and drag the cursor over the text. Then simply type in the replacement text. The replacement text will appear in a commenting box. You may also cut-and-paste text from another file into this box. To replace formatted text (an equation for example) please Attach a file (see below).
Remove text	Click the 'Text Edits' button  on the Commenting tool bar. Click and drag over the text to be deleted. Then press the delete button on your keyboard. The text to be deleted will then be struck through.	Click the 'Strikethrough (Del)' icon  on the Comment tool bar. Click and drag over the text to be deleted. Then press the delete button on your keyboard. The text to be deleted will then be struck through.
Highlight text/ make a comment	Click on the 'Highlight' button  on the Commenting tool bar. Click and drag over the text. To make a comment, double click on the highlighted text and simply start typing.	Click on the 'Highlight Text' icon  on the Comment tool bar. Click and drag over the text. To make a comment, double click on the highlighted text and simply start typing.
Attach a file	Click on the 'Attach a File' button  on the Commenting tool bar. Click on the figure, table or formatted text to be replaced. A window will automatically open allowing you to attach the file. To make a comment, go to 'General' in the 'Properties' window, and then 'Description'. A graphic will appear in the PDF file indicating the insertion of a file.	Click on the 'Attach File' icon  on the Comment tool bar. Click on the figure, table or formatted text to be replaced. A window will automatically open allowing you to attach the file. A graphic will appear indicating the insertion of a file.
Leave a note/ comment	Click on the 'Note Tool' button  on the Commenting tool bar. Click to set the location of the note on the document and simply start typing. <u>Do not use this feature to make text edits.</u>	Click on the 'Add Sticky Note' icon  on the Comment tool bar. Click to set the location of the note on the document and simply start typing. <u>Do not use this feature to make text edits.</u>

HOW TO...		
Action	Adobe Reader version 9	Adobe Reader version X and XI
Review	To review your changes, click on the 'Show' button  on the Commenting tool bar. Choose 'Show Comments List'. Navigate by clicking on a correction in the list. Alternatively, double click on any mark-up to open the commenting box.	Your changes will appear automatically in a list below the Comment tool bar. Navigate by clicking on a correction in the list. Alternatively, double click on any mark-up to open the commenting box.
Undo/delete change	To undo any changes made, use the right click button on your mouse (for PCs, Ctrl-Click for the Mac). Alternatively click on 'Edit' in the main Adobe menu and then 'Undo'. You can also delete edits using the right click (Ctrl-click on the Mac) and selecting 'Delete'.	To undo any changes made, use the right click button on your mouse (for PCs, Ctrl-Click for the Mac). Alternatively click on 'Edit' in the main Adobe menu and then 'Undo'. You can also delete edits using the right click (Ctrl-click on the Mac) and selecting 'Delete'.

SEND YOUR ANNOTATED PDF FILE BACK TO ELSEVIER

Save the annotations to your file and return as instructed by Elsevier. Before returning, please ensure you have answered any questions raised on the Query Form and that you have inserted all corrections: later inclusion of any subsequent corrections cannot be guaranteed.

FURTHER POINTS

- Any (grey) halftones (photographs, micrographs, etc.) are best viewed on screen, for which they are optimized, and your local printer may not be able to output the greys correctly.
- If the PDF files contain colour images, and if you do have a local colour printer available, then it will be likely that you will not be able to correctly reproduce the colours on it, as local variations can occur.
- If you print the PDF file attached, and notice some 'non-standard' output, please check if the problem is also present on screen. If the correct printer driver for your printer is not installed on your PC, the printed output will be distorted.

Structured Synaptic Connectivity between Hippocampal Regions

Shaul Druckmann,^{1,5} Linqing Feng,^{2,5} Bokyoung Lee,^{2,3} Chaehyun Yook,^{2,4} Ting Zhao,¹ Jeffrey C. Magee,^{1,*} and Jinhyun Kim^{2,*}

¹Janelia Farm Research Campus, Howard Hughes Medical Institute, 19700 Helix Drive, Ashburn, Virginia 20147, USA

²Center for Functional Connectomics, Korea Institute of Science and Technology (KIST), 39-1 Hawolgokdong, Seoul, 136-791, Korea

³Neuroscience program, University of Science and Technology, 176 Gajeongdong, Daejeon, 305-350, Korea

⁴Department of Biological Science, KAIST, 373-1 Guseongdong, Daejeon, 305-701, Korea

⁵These authors contributed equally to this work

*Correspondence: mageej@janelia.hhmi.org (J.C.M.), kimj@kist.re.kr (J.K.)

<http://dx.doi.org/10.1016/j.neuron.2013.11.026>

SUMMARY

The organization of synaptic connectivity within a neuronal circuit is a prime determinant of circuit function. We performed a comprehensive fine-scale circuit mapping of hippocampal regions (CA3-CA1) using the newly developed synapse labeling method, mGRASP. This mapping revealed spatially nonuniform and clustered synaptic connectivity patterns. Furthermore, synaptic clustering was enhanced between groups of neurons that shared a similar developmental/migration time window, suggesting a mechanism for establishing the spatial structure of synaptic connectivity. Such connectivity patterns are thought to effectively engage active dendritic processing and storage mechanisms, thereby potentially enhancing neuronal feature selectivity.

INTRODUCTION

The active properties of dendrites allow neurons to respond selectively to specific spatiotemporal patterns of synaptic input (Branco et al., 2010; Gasparini and Magee, 2006; Poirazi et al., 2003; Polsky et al., 2004; Spruston, 2008). Spatially nonuniform input, where individual dendritic branches receive disproportionate synaptic input, is particularly effective at engaging dendritic boosting and plasticity mechanisms (Harvey and Svoboda, 2007; Losonczy et al., 2008). This active dendritic processing is thought to enhance the ability of neural circuits to detect higher-order features that could be embedded within the structure of the synaptic input (Lavzin et al., 2012; Legenstein and Maass, 2011; Poirazi et al., 2003; Polsky et al., 2004; Ujfalussy and Lengyel, 2011).

Despite its potential functional importance there remains a good deal of uncertainty about the level of structure in the subcellular connectivity patterns within many neural circuits. It is, however, increasingly evident that connectivity patterns among some pre- and postsynaptic neurons are not random. On a macroscopic scale it is clear that at a minimum the probability of connection is dependent on neuronal identity (Brown and Hestrin, 2009; Deguchi et al., 2011; Li et al., 2012; Yu et al., 2009)

and, on a finer scale, functionally similar inputs appear to cluster together onto specific dendritic branches (Kleindienst et al., 2011; Makino and Malinow, 2011; McBride et al., 2008; Takahashi et al., 2012). Nonetheless, the spatial connectivity patterns between central neurons remain only loosely characterized and some data have been interpreted to indicate that input patterns onto principal neurons in several neocortical areas are poorly structured or even random (Jia et al., 2010; Varga et al., 2011).

To directly determine the degree and nature of spatial structure within a given synaptic input path, we used mammalian GFP reconstitution across synaptic partners (mGRASP) with an improved computational analysis to precisely map the spatial profile of the main excitatory synaptic CA3 input to hippocampal CA1 pyramidal neurons (Feng et al., 2012; Kim et al., 2012). We found that the density of synapses on different dendritic branches within single CA1 neurons was highly variable and strongly deviated from that expected from a spatially uniform input. In addition, we detected an overabundance of small intersynapse distances between consecutive synapses on a given dendritic branch. Such synaptic clustering was more prevalent between groups of neurons that had developed at the same time, suggesting a potential mechanism for establishing this subcellular spatial structure.

RESULTS

Variable Synaptic Connectivity at the Cellular Level

We first examined synaptic contacts between broad populations of presynaptic CA3 neurons and individual postsynaptic CA1 pyramidal neurons to generally characterize the connectivity ($n = 32$ neurons, 5 mice). The morphologies of sparsely labeled postsynaptic CA1 neurons and their synapses with broadly labeled presynaptic CA3 neurons were then determined through neuTube-assisted tracing and mGRASP image analysis techniques as previously described (see [Experimental Procedures](#), [Figures 1A](#) and [1B](#), and [Movies S1](#), [S2](#), and [S3](#)) (Feng et al., 2012; Kim et al., 2012). Finally, we analyzed the distribution of synapses, testing for different forms of statistically significant structure within those distributions ([Figure S1A](#), available online).

Synapses were evident throughout the CA1 basal and apical dendrites except for the apical tuft dendrites, which are known to lack inputs from CA3 ([Figure S2](#)). The number of synapses

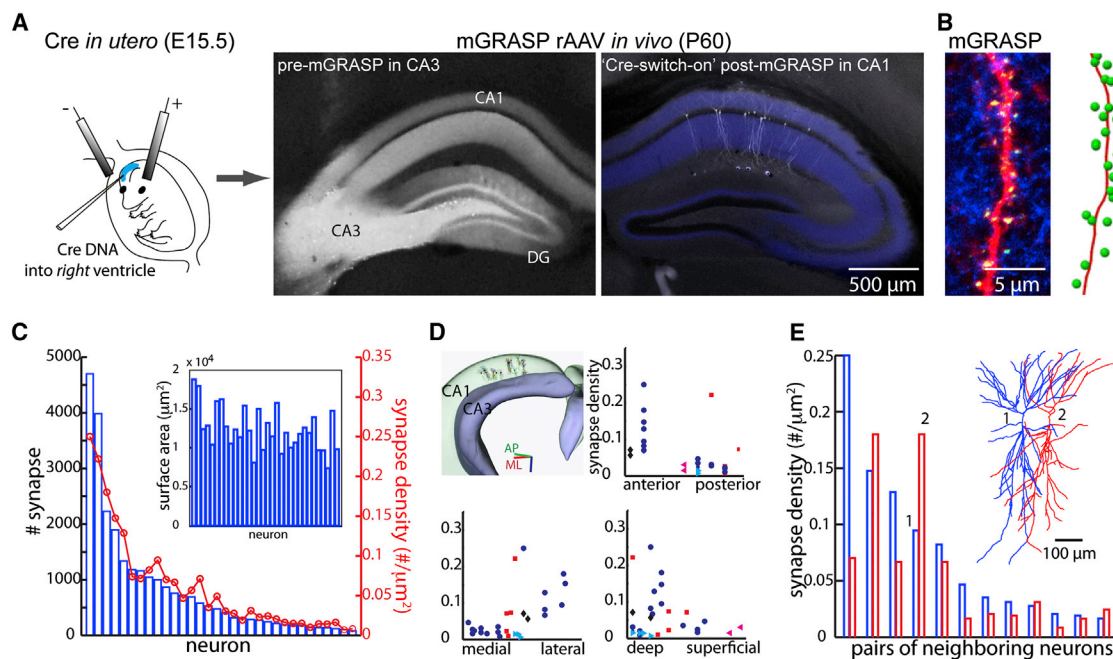


Figure 1. Variable Synaptic Connectivity at the Cellular Level

(A) Strategy for mGRASP expression to study hippocampal CA3-CA1 synaptic connectivity pattern. Broad presynaptic CA3 and sparse postsynaptic CA1 labeling: the plasmid containing iCre recombinase was transfected into CA1 progenitor cells of the right ventricle via in utero electroporation on embryonic day 15.5 (E15.5). Cre-independent pre-mGRASP and Cre-dependent “switch on” post-mGRASP rAAV were injected into left CA3 and right CA1, respectively, on postnatal day 60~75. Example fluorescent images show dense axonal projection of CA3 neurons expressing pre-mGRASP (left) and sparse CA1 neurons expressing post-mGRASP in white along with dense CA3 axonal projections in blue (right).

(B) Example dendrite showing a number of reconstituted mGRASP signals (green) in sites where dense CA3 axons (blue) intersect with a CA1 dendrite (red) (left) and its neuTube-reconstruction with detected mGRASP puncta (right).

(C) Sorted bar plot shows highly variable number of synapses per neuron across population ($828 \pm 1,065$ [mean \pm STD], per neuron, range 83–4,701). Overlaid red graph indicates synaptic density and inset shows surface area of each neuron (surface area: $12,365 \pm 2,767 \mu\text{m}^2$, range 7,371–18,792; synaptic density: $0.061 \pm 0.06 \text{ synapse}/\mu\text{m}^2$, range 0.007–0.25).

(D) Spatial location of postsynaptic CA1 neurons among 3D hippocampal landmarks (top left) and scatter plot of synaptic density versus spatial location. Different colors and markers indicate different animals. Anterior-posterior ranged $-2.0 \sim -2.8$ mm from bregma (binned from 100- μm -thick slices), medial-lateral ranged 1~2.25 mm, and depth ranged 1~1.27 mm from dura. AP: anterior-posterior, ML: medial-lateral.

(E) Comparison of synaptic density of nearest-neighbor pairs in a single animal shows variable number of synapses per neuron within a single animal. The synaptic density of the first (blue) and second (red) neuron of the pair is shown, sorted by the density of the first pair member. Inset shows two neuTube-reconstructed neurons marked by 1, 2. See also Figure S1, Figure S2, and Movies S1, S2, and S3.

per neuron was highly variable (Figure 1C). This variability was not due to diversity in neuron morphology since the dendritic surface area in our sample varied considerably less than the synaptic density (Figure 1C). We also found moderate differences in synaptic density along the anterior-posterior axis (anterior increased density, $p < 0.03$ Wilcoxon rank-sum test) and the medial-lateral axis (lateral increased density, $p < 0.04$), consistent with the previously reported large-scale axonal projection patterns in rats (Figure 1D) (Ishizuka et al., 1990; Li et al., 1994). However, these topographical differences were too small to fully explain the cell-to-cell variability in synaptic density. Between-animal differences in synapses also could not fully explain the variation in density since synaptic density varied more than 5-fold within individual animals. In fact, even nearest-neighbor neurons in the same animal varied considerably in synaptic density (Figure 1E), ruling out both topographical and animal-to-animal differences as sole sources of variability. The variability in synaptic distribution was also observed at the level of branch

subclasses (Figure S2). In sum, we found that the CA3 presynaptic population does not uniformly innervate the CA1 pyramidal postsynaptic population.

Structured Synapse Distribution at the Branch Level

We next examined the spatial structure of synaptic connections among the different dendrites of single neurons (Figure S1B) and found substantial variability in the synaptic densities of individual branches of a given neuron (Figure 2A). To relate the actual, measured branch-level variability to that expected by chance we compared our observations to those generated by the control, spatially random hypothesis, i.e., a Poisson process predicting numbers of synapses for a given dendritic area. The degree of deviation between measured and chance ranged from large (Figure 2A) to small (Figure 2B) differences among individual basal branches. On the population level, we found significant variations in synaptic density in individual basal branches of most neurons (22 significant out of 28

Neuron

Structured Synaptic Connectivity

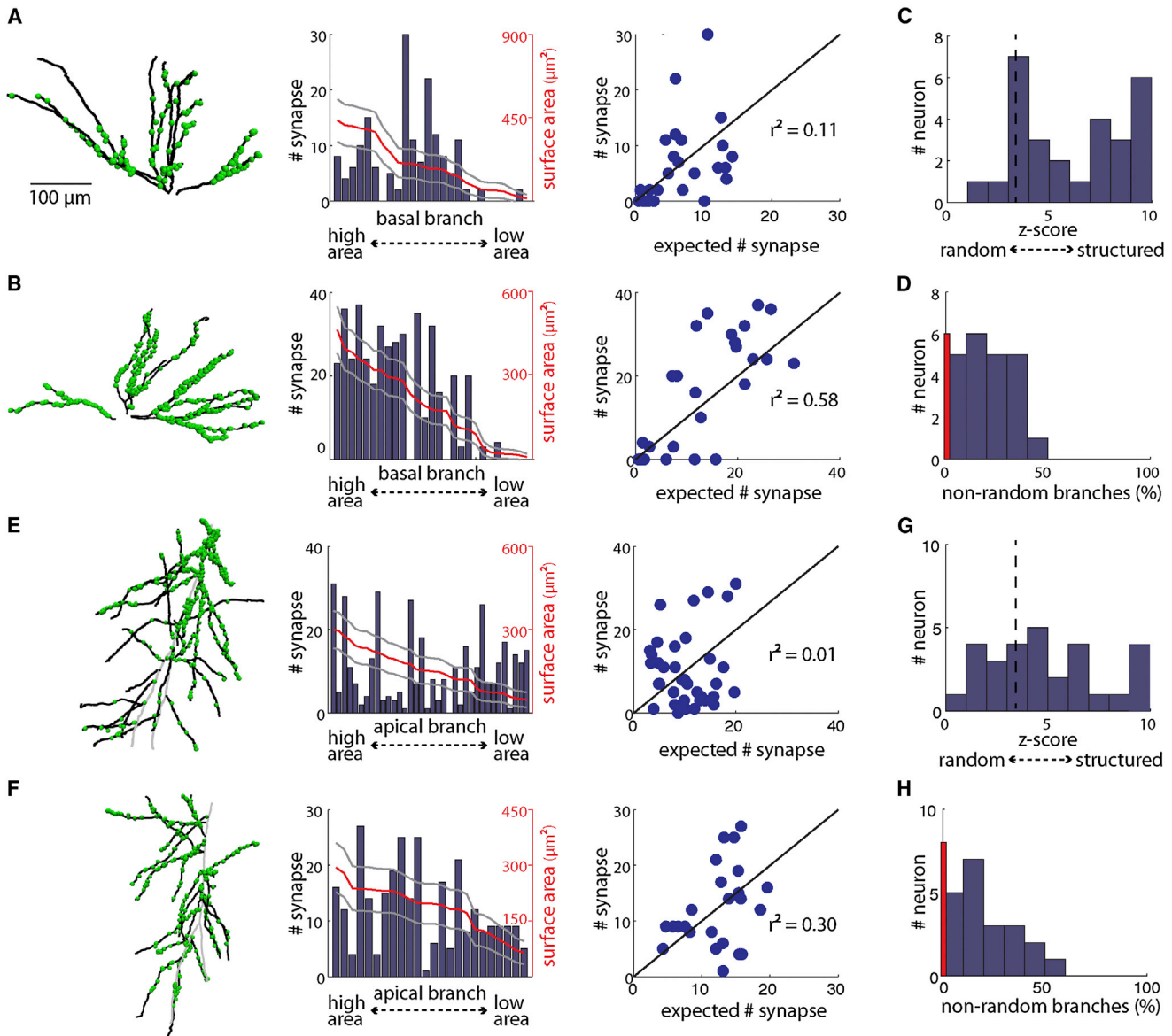


Figure 2. Random versus Structured Synapse Distribution at the Branch Level

(A) Example of structured synaptic distribution on CA1 basal dendrites. Synapses detected by mGRASP are presented as green dots on neuTube-traced branches (left). Bar plot shows the number of synapses on each basal branch, while overlaid red line indicates the surface area of each branch (right y axis) and number of synapses expected in a control Poisson distribution (left y axis); gray lines indicate ± 1 SD of synapse number. Branches are sorted according to their surface area (middle). Relation between actual number of synapses and expected number of synapses in control model is shown in scatter plot (right).

(B) Example of nearly random synaptic distribution on basal dendrites is shown as in (A).

(C) Histogram of maximal deviation from random Poisson distribution of basal branches for each neuron indicates variability in degree of structured synaptic distribution on basal branches. Deviation is determined by Z score distance from the expected number of synapses. Average threshold of significance indicated by dashed line.

(D) Histogram of fraction of basal branches with significant deviations from chance.

(E–H) Structured and random synaptic distribution on apical oblique dendrites is presented as in (A)–(D). Main trunk branches, shown in gray, were excluded from this analysis. See also Figure S1.

neurons considered, 4 neurons were excluded from the 32 for this analysis due to low synapse number, Figures 2C and 2D). Radial oblique and basal dendrite arbors were considered separately and similar levels of variation in the synaptic density

of individual dendritic branches were found for both arbor regions (Figures 2E–2H). In addition, nonrandom distributions were also observed when branches were defined according to electrical signal path of a branch, which concatenates all

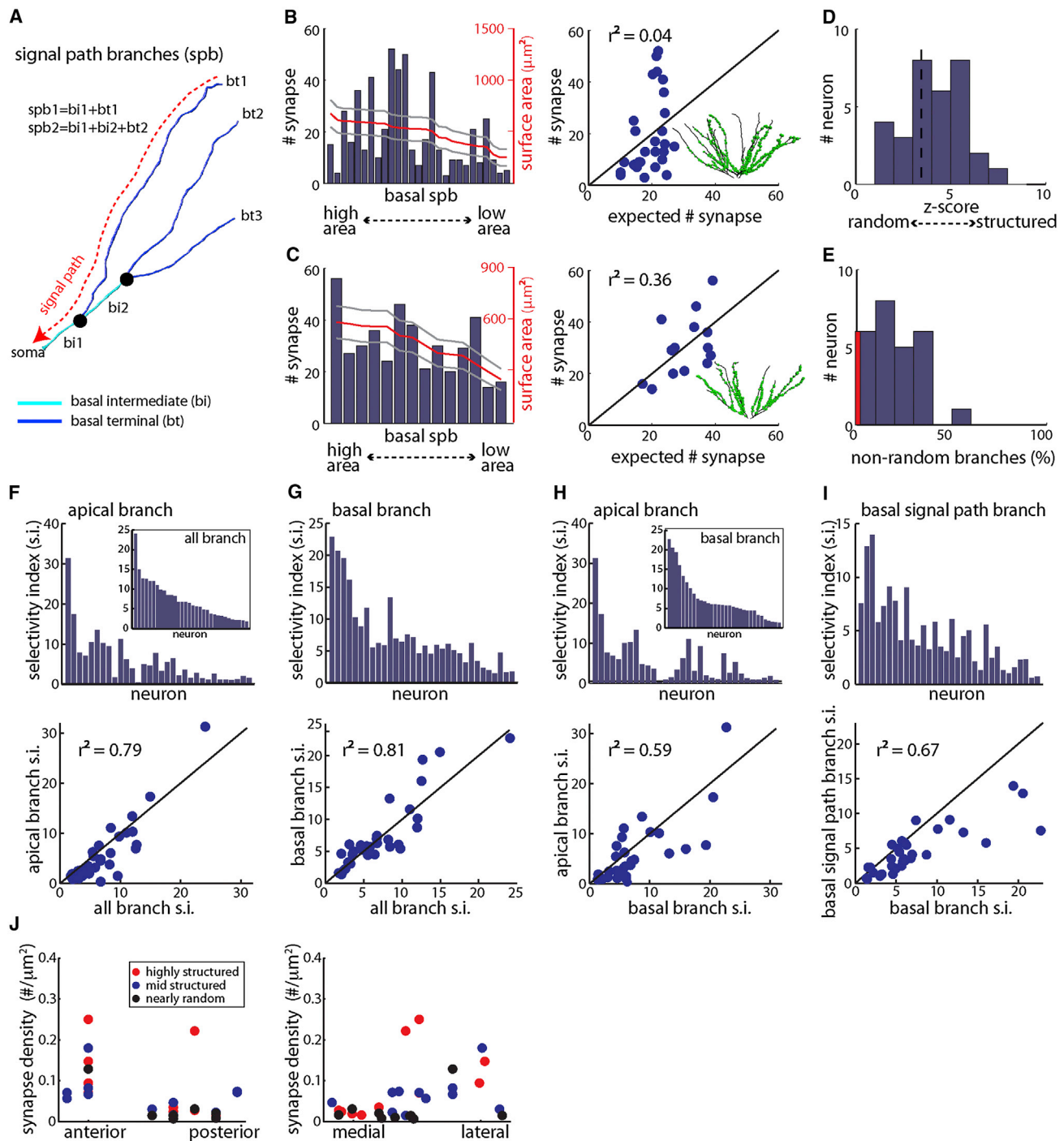


Figure 3. Structured Synapse Distribution of Different Branch Types

(A) Scheme of subclassification of basal dendrites considering electric signal path from branch tips to the soma.

(B) Example of structured synaptic distribution on CA1 basal signal path branches (spb). Bar plot shows the number of synapses on each basal signal path branch, while overlaid red line indicates the surface area of each branch (right y axis) and expected number of synapses in control Poisson distribution (left y axis), and gray lines indicate ± 1 SD of synapse number. Branches are sorted according to their surface area. Relation between actual number of synapses and expected number of synapses in control model is shown in scatter plot (right). Synapses detected by mGRASP are presented as green dots on neuTube-traced branches (right inset).

(C) Example of nearly random synaptic distribution on basal signal path branches shown in the same format as in (B).

(D) Histogram of maximal deviation from expected number of synapses. Deviation is determined by Z score distance from the expected number of synapses. Average threshold of significance indicated by dashed line.

(legend continued on next page)

the branches along the path from a specific terminal branch toward the soma (Losonczy and Magee, 2006) (Figures 3A–3E). Indeed, neurons whose synaptic distributions showed stronger deviations from randomness in the basal dendrites were also more likely to have stronger deviations in oblique dendrites (Figures 3F–3I). Finally, no obvious relationship between topographic location and degree of structure was found (Figure 3J). These results clearly demonstrated branch-level structure of synaptic connectivity, i.e., that many branches were either more or less heavily innervated than would be expected by chance.

Validation of mGRASP for Branch-Level Synapse Distribution

We performed a number of controls to ensure the validity of our finding of branch-level structure of synaptic distribution. First, we considered the possibility that the branch-level structure we found above in mGRASP-labeled synapse distribution is due to variability in the total number of all synapses upon each branch, and not due to spatially nonuniform connectivity as we suggested above. We found that the total putative synapse density, determined by counting the number of spines present on a given branch, was comparable on terminal branches with both high and low densities of mGRASP-labeled synapses (Figures 4A–4C). Unlike the number of mGRASP-labeled synapses, the total number of spines on a branch was very well described by the branch length and the nonrandom structured synapse distribution at the branch level held true when spine density was analyzed instead of branch length (Figures 4C and 4D). These observations are consistent with other reports that synapse density among the different dendritic branches of CA1 pyramidal neurons is relatively constant (Banister and Larkman, 1995; Megias et al., 2001; Nicholson et al., 2006).

We next addressed a second concern, that the variability in synapse number is driven by variability in postsynaptic expression of mGRASP component. Although our analysis is not overly sensitive to low levels of variability in the translocation of the postsynaptic mGRASP component from branch to branch or synapse to synapse (see [Experimental Procedures](#)) we used immunostaining techniques to quantify that postsynaptic mGRASP was indeed uniformly present at all dendritic branches and in most (approximately 97%) synapses (Figure 5 and [Movie S4](#)). This analysis demonstrates that the broadly labeled population of CA3 pyramidal neurons does not uniformly innervate the different dendrite branches of most CA1 pyramidal neurons.

Branch-Level Variability Is Not Explained by Axonal Variability

We next tested whether the branch-level variability in synapse density is explained by the variability of available presynaptic axonal density. Specifically, we started by considering the hypothesis that the number of synapses on a branch is proportional to the product of the postsynaptic dendritic surface area and the presynaptic axonal density, a widely accepted hypothesis known as Peters's rule (Peters and Feldman, 1976). Reanalyzing our data by applying this rule rather than by relying on dendritic surface area alone did not improve the match of measured to predicted synapse number (Figure 6A). Directly testing the hypothesis we found no significant linear correlation between axonal and synaptic density in any of the 28 neurons on both single-neuron and population levels (Figures 6A, 6B, and S3). We next tested the correspondence between axonal and synaptic density more generally than the simple linear product relationship (Figures 6C–6F). Allowing for different linear relationships between axonal and synaptic density among basal or apical branches only modestly increased the explained variance (3%, Figure S3) with only a small fraction of neurons (2 of 28) showing a significant correlation. We did, however, find significant corresponding changes in axonal density for those branches that had lower-than-expected synapse numbers (Figure 6E) and this relation was most reliable between branches with extremely low synapse density and very little to no surrounding axonal density (<5% of max, Figure 6F). Branches with greater-than-expected synaptic densities had somewhat higher mean axonal density compared to branches with expected synaptic density, but the difference did not reach significance. In summary, these results show that simple relationships between synaptic and axonal density, as suggested for instance by Peters's rule, explains little of the branch-to-branch variability we observed in synaptic density (Mishchenko et al., 2010). Taken together, all the data presented in the sections above suggest that there exists a high degree of biasing in the branch-level innervation pattern of the presynaptic population of CA3 neurons, with some branches preferentially contacted at the expense of other branches.

Clustered Synaptic Connectivity

Recent reports describe locally synchronous synaptic activity (Makino and Malinow, 2011; Takahashi et al., 2012), suggesting a sub-branch-level structure in the connectivity. Accordingly, we next examined intrabranch specificity or "synaptic clustering" (Figures 7 and S1C). Given a hypothesis of spatially random Poisson distribution of synapses across a branch, the

(E) Histogram of fraction of signal path branches that show significant deviations from control model demonstrates both random and selective neurons, similarly to subclass branch analysis.

(F–I) Relation between selectivity and branch type. (F) Branch-level synaptic selectivity index (s.i.) was determined as the degree of variability of synaptic density on branches. Each bar corresponds to the selectivity index of a single neuron. Synaptic selectivity index was calculated for apical oblique branches only (top) and neurons were sorted by the full neuron selectivity index (inset). Scatter plot of selectivity between apical oblique branches against all branches (bottom). (G) Same analysis as (E) but for basal branches only. (H) Synaptic selectivity index of apical branches (top) sorted by the basal branch selectivity index (inset). Scatter plot of selectivity between basal branches against apical oblique branches shows weaker correspondence than in (F) and (G) (bottom). (I) Synaptic selectivity index of basal signal path branches (top) sorted by the technical branch selectivity index (inset of H). Scatter plot of selectivity between technical branches against signal path branches shows midstrength correspondence between technical and signal path branch selectivity (bottom).

(J) No clear pattern of degree of synaptic structure in topographic location. Neurons were divided into three groups based on selectivity index of total branches, i.e., a highly structured (red), a midstructured (blue), and a nearly random neuron (black), and shown in plots of their total synaptic density and spatial location.

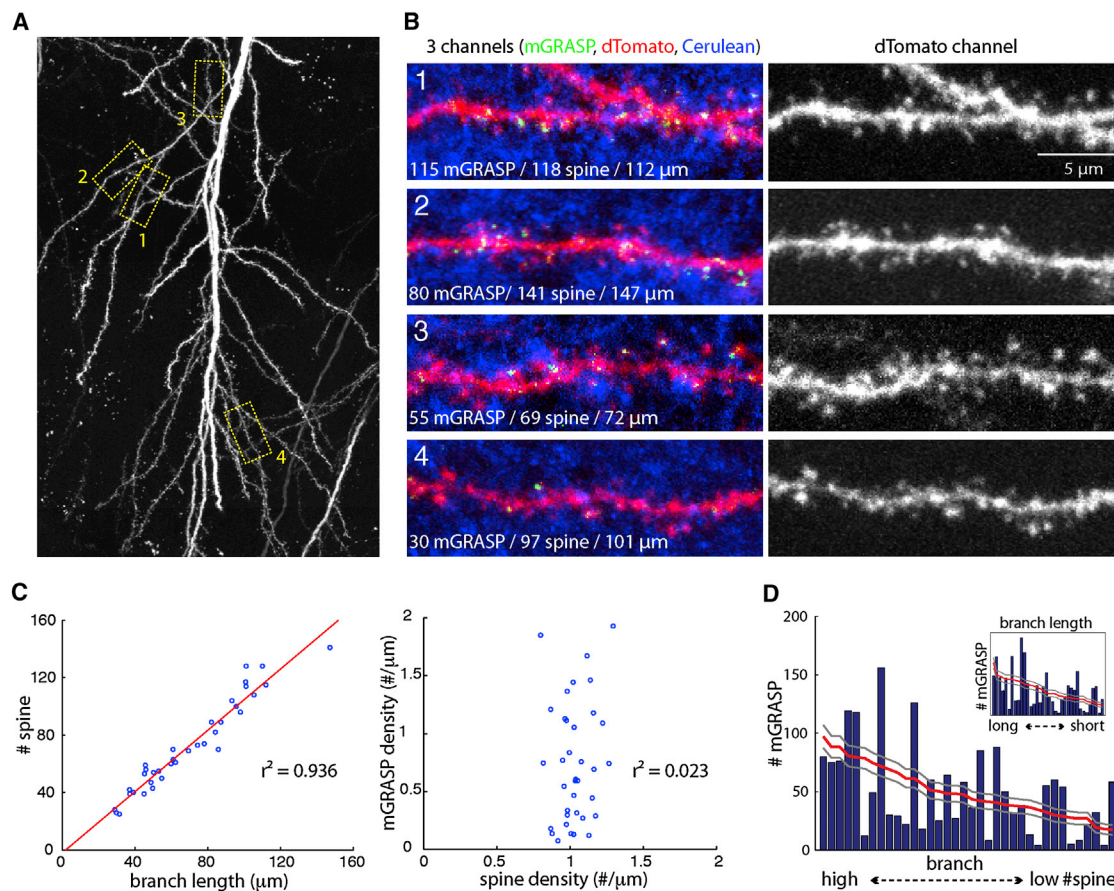


Figure 4. Analysis of Putative Synapse and mGRASP-Positive Synapse Density

(A) Overview of spiny apical dendrites of a CA1 neuron expressing post-mGRASP and dTomato.

(B) High-magnification images of example dendrites indicated by dashed boxes 1–4 in (A) show that the putative synapse density is consistent in dendrites, while mGRASP-positive synapse density varies even in sister branches (1 and 2). Putative synapse number was determined by counting only spines that appeared on the lateral sides of branches since the low z resolution of LM hindered accurate counting of spines at other orientations since they become superimposed on dendrites.

(C) The strong linear relation between the dendritic length and the spine number of oblique terminal branches (right, $n = 36$, $p = 6.6 \times 10^{-22}$) and the weak relation between mGRASP-positive synapse and spine density (left, $p = 0.38$) are shown in scatter plots. Average of the spine density of these branches is $1.03 \pm 0.02/\mu\text{m}$, approximately one-third of the EM-determined spine density (Bannister and Larkman, 1995; Megias et al., 2001; Nicholson et al., 2006) since only laterally appearing spines, not ones superimposed upon branches, were counted because of the low z resolution of LM.

(D) Bar plots show the number of mGRASP-positive synapses on each apical terminal branch of (A), while overlaid red line indicates expected number of synapses in control Poisson distribution. Branches were sorted according to their spine number and length (inset).

distances between consecutive synapse locations along the branch should follow an exponential distribution. We found that many neurons (17 of 27, 5 neurons were excluded because they had too few synapses) had branches with significant deviations from the expected distribution (see [Experimental Procedures](#)). The most pronounced difference was an overabundance of small intersynapse distances, consistent with clustering (Figure 7A). To complement this analysis we generated multiple control random synaptic placements and compared them to the real synaptic locations. Consistent with the results above, we found that the distribution of nearest neighbor synapse distances was shifted to shorter distances than expected by chance, though the distributions partially overlapped (Figure 7B). We next operationally defined a cluster as a pair of synapses separated by less than $1.5 \mu\text{m}$ and found

that neurons had more clusters than expected by chance (Figure 7C) with the fraction of significantly clustered branches varying from neuron to neuron (Figure 7D). Similar patterns were found when apical and basal arbors were considered separately (Figure S4). These results point to an unexpected degree of synaptic clustering.

A cluster can result either from multiple, different axons creating synapses in close proximity or from multiple synapses formed by the same, single axon. The limitations of light microscopy prevent us from tracing single axons with the necessary confidence; thus, we cannot distinguish between these two possible sources of synapse clustering. However, by estimating the number of axons given the distribution of single-axon multiple contacts reported (Sorra and Harris, 1993), we extrapolate that single-axon multiple contacts may account for up to half

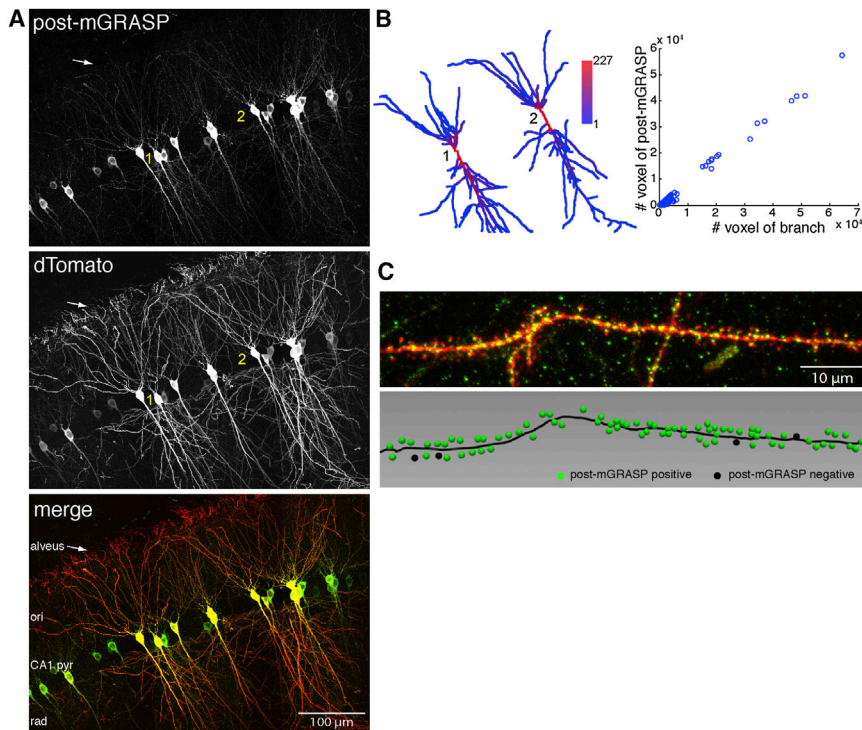


Figure 5. No Branch- or Synapse-Specific Expression of Post-mGRASP Component

(A) Spatial distribution of post-mGRASP component visualized by anti-GFP immunolabeling followed by anti-DsRed staining is nearly ubiquitous along dendrites. No or little signals in alveus (arrow) where axons of CA1 neurons pass indicate postsynaptic expression of designed post-mGRASP component.

(B) Color map of intensity of post-mGRASP component (left, reconstructed neurons 1 and 2 from A and strong correlation between the voxel number of branches and post-mGRASP positive; right, 385 branches from 5 neurons, Spearman's $\rho = 0.86$, $p < 0.0001$) shows little variation in expression of post-mGRASP component along branch by branch.

(C) High-magnification image and its reconstruction show no synapse-specific expression of post-mGRASP component. See also [Movie S4](#).

of the difference between expected and actual number of clusters (566/1095, see [Experimental Procedures](#)).

Enhanced Structure of Synaptic Connectivity between Temporally Matched Neurons

Our analysis thus far revealed multiple levels of structured input patterns. A natural hypothesis is that these structured connectivity patterns may be linked to variations in the population of labeled neurons. Indeed, specific connectivity has been previously observed among principal neurons that share a particular neurogenesis and synaptogenesis time window. These “temporally matched neurons” form distinct subpopulations and show elevated probabilities of synaptic connectivity ([Deguchi et al., 2011](#); [Yu et al., 2009](#)). To investigate this possibility we collected a second set of data consisting of temporally matched hippocampal pre- and postsynaptic neuronal subpopulations ([Figures 8A and 8B](#) and [Movie S5](#)). By in utero transduction of rAAV expressing Cre recombinase to CA3 and CA1 progenitor cells in both ventricles (E15.5) and sequential stereotaxic injection of Cre-dependent “switch-on” pre- and post-mGRASP rAAV into left CA3 and right CA1 (P60~75), respectively, we labeled synapses between specific temporally matched subpopulations of CA3 and CA1 cells. Although we observed fewer synapses per neuron in this temporally matched set (average 25.7 ± 20.4 , range: 7–88, $n = 20$ neurons, 3 animals), we found significantly more connections between temporally matched neurons than expected by chance ([Deguchi et al., 2011](#)): (temporally matched labeling: 0.2 synapses per presynaptic cell, presynaptic cell number range 103–193, [Figure 8C](#); broad labeling: average synapses per presynaptic cell 0.035 based on estimate of 25,000 presynaptic CA3 neurons, comparison to temporally

matched data $p < 1 \times 10^{-5}$, Wilcoxon rank sum test; 0.07 synapses per presynaptic neuron based on 50,000 presynaptic neurons, comparison $p < 1 \times 10^{-6}$). Furthermore, synaptic clustering was highly pronounced in this data set ([Figures 8D–8F](#)). In one characteristic example neuron ([Figures 8D and 8F](#)) we found three synaptic pairs among only ten synapses on the entire tree, a distribution very unlikely to occur by chance ($p < 0.00001$, Monte Carlo estimation). As a population, the number of clusters was approximately ten times greater than expected by chance and nearly five times greater than that found in the set of broadly labeled neurons described earlier (compare [Figure 8F](#) to [Figure 7C](#)). Significant clustering was observed in most temporally matched neurons, most commonly as synaptic pairs. Estimating the number of single-axon multiple contacts as above, we find that they can account for up to ~30% of the unexpected synapses (15/52). Even if one assumes that all the extra clusters in the dense data set were from axons making multiple synaptic contacts (yielding an estimate twice as high as that reported [[Sorra and Harris, 1993](#)], 9.8%), the sparse data set would still have 20 unexpected clusters. To fully account for all the unexpected clusters in the sparse data set, the fraction of multiple synaptic contacts would need to be set nearly five times as high (19.5%) as that reported ([Sorra and Harris, 1993](#)). All in all, we find that structured connectivity, as measured by synaptic density and clustering, is enhanced among temporally matched hippocampal neurons.

DISCUSSION

We found that the synaptic connectivity profile between hippocampal CA3 and CA1 pyramidal neurons strongly deviated from randomness at all three levels of our analysis: neuron, branch, and subbranch. Because these results demonstrate that a linear relationship between synaptic and axonal density explains little of the variance in synaptic density between

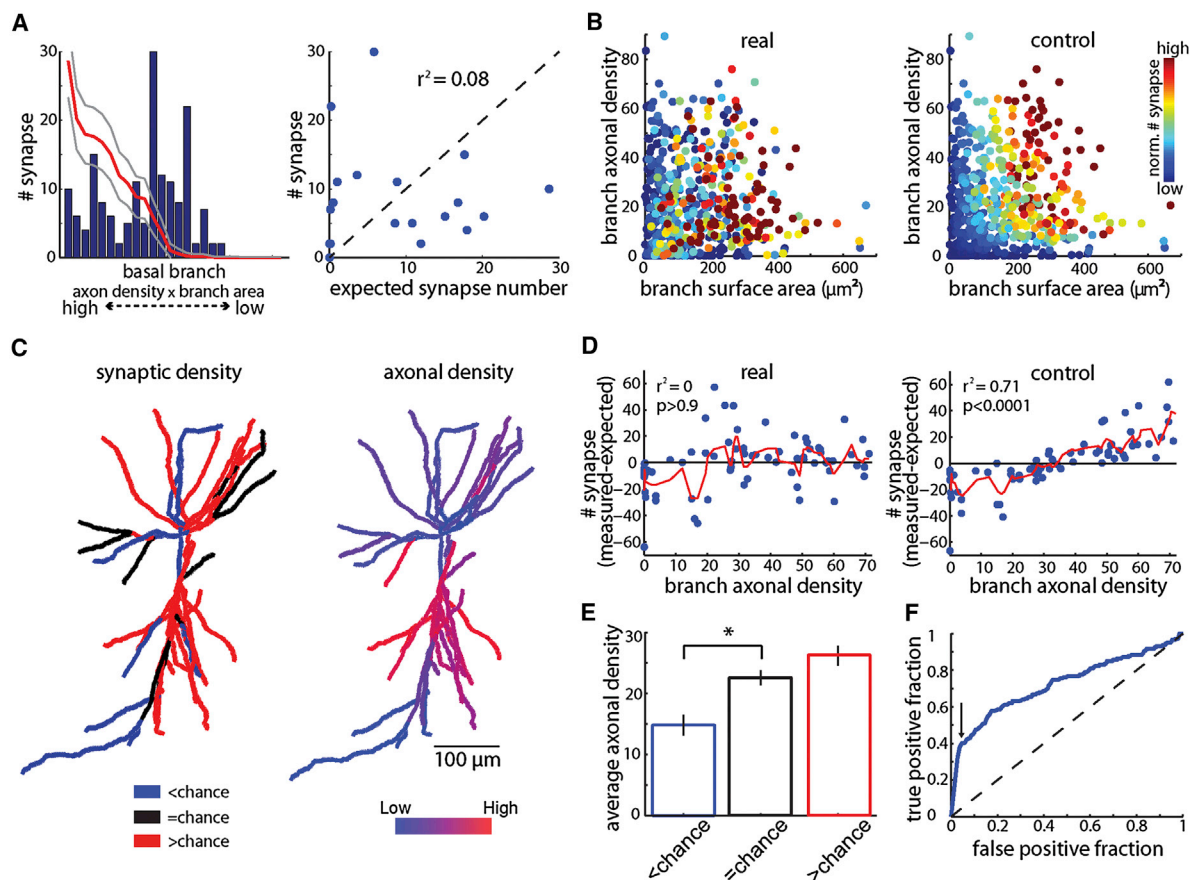


Figure 6. Weak Correlation between Synaptic Density and Available Axon Density

(A) Relation of Peters's rule prediction to number of synapses in single neuron. Bar plot shows the number of synapses on each basal branch for the neuron shown in Figure 2A, while overlaid red line indicates the expected number of synapses in control Poisson distribution (left y axis); gray lines indicate ± 1 SD of synapse number. Branches are sorted according to their Peters's rule value, i.e., the product of axon density and branch surface area (left). Relation between actual number of synapses and expected number of synapses in control model is shown in scatter plot (right).

(B) Population level relation of Peters's rule prediction to synapse number. Color plot shows each branch as a dot with a color corresponding to the number of synapses at an x axis location corresponding to branch's surface area and y axis location corresponding to the axonal density for real data (left), and control model where synapse number was generated according to Peters's rule (right). Number of synapses was normalized to the synapse density of the neuron of origin to allow population aggregation despite differences in synaptic density between neurons.

(C) Synaptic density of dendrites with respect to control Poisson model where branches in blue and red show significantly less and more synaptic density than chance, respectively, while those in black are not significantly different from chance (left). Heat-map of axonal density surrounding the branches (right).

(D) Relation of axonal density to difference between actual synapse number and expected synapse number for the neuron shown in (C). Each dot represents a branch and overlaid red line indicates local average values of difference of synapse (left). The scattered nonmonotonic average values indicate deviation from Peter's rule, contrasted with the linear relation in an artificial synapse placement model which follows Peter's rule (right).

(E) Averaged axonal density of three branch groups sorted from 32 neurons, grouped and color coded as in (A), demonstrates that synaptic density more strongly correlates with axonal availability at the branch level in the case of low synaptic density ($p < 0.01$ Wilcoxon rank sum test). Error bars indicate SEM.

(F) Consistent with (E), receiver operating characteristic (ROC) analysis, predicting whether a branch has significantly fewer synapses than chance given axonal density, shows that prediction of low synaptic density from axonal density is accurate with few false positives. Arrow indicates point of high reliability. See also Figure S3.

branches, they call into question Peters's rule. Together, our data indicate that there is a high degree of spatial structure or selectivity present within the Schaffer collateral inputs to CA1 pyramidal neurons that may at least partially result from special connectivity patterns among subpopulations of principal neurons that developed together. These new data from CA1 are congruent with previous reports that indicate the presence of clustered types of input patterns in other brain regions (Kleindienst et al., 2011; Makino and Malinow, 2011; McBride et al.,

2008; Takahashi et al., 2012) but contrast with those reported for several cortical principal neurons (Jia et al., 2010; Varga et al., 2011). These differences may be the result of the different technical approaches employed in these studies or from actual dissimilarities in the various circuits. Indeed, it is not expected that all neuronal microcircuits will use the same information-processing strategies. For instance, dentate granule cells, which are only two stages before CA1, do not appear to possess the intrinsic capability to respond to structured input patterns,

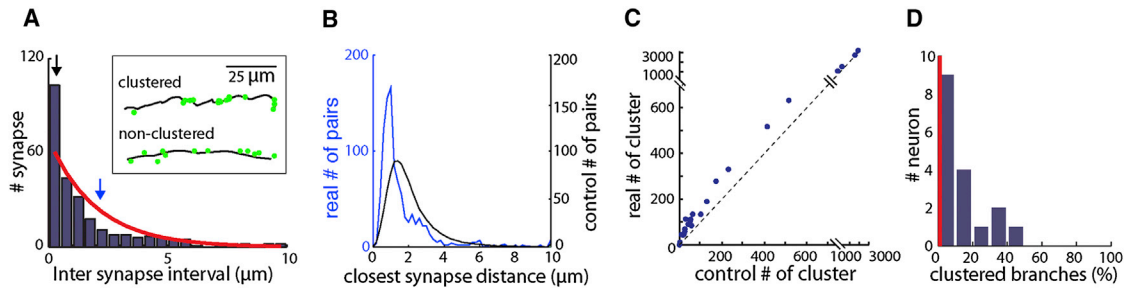


Figure 7. Clustered Input Connectivity from Broad Labeled Presynaptic CA3

(A) Histogram of intersynapse distance along branch for clustered branches. Overlaid red line indicates control exponential distribution. Result shows greater than expected number of small intersynapse distances (marked by black arrow) and a corresponding decrease in medium distance intersynapse distances (marked by blue arrow). Inset: magnified view of clustered and nonclustered branches.

(B) Distribution of nearest neighbor synapse distances for measured results (blue) shows more synaptic clusters than the expected distribution in random control model (black).

(C) Scatter plot of the expected number of clusters separated by less than 1.5 μm , in control model against the actual number of clusters in the data shows more clusters than expected by chance ($p < 0.00001$ Monte Carlo estimation). Each dot represents a neuron.

(D) Histogram of the number of neurons with a given fraction of significantly clustered branches ($p < 0.00001$ Monte-Carlo estimation) shows variability of clustering. Red bar at zero indicates the number of neurons with no significantly clustered branches. See also [Figures S1 and S4](#).

suggesting that they might not receive such patterns (Krueppel et al., 2011). It remains an interesting open question as to whether there is a direct link between the processing capabilities of various principal neurons, the level of structured connectivity present within their input pathways, and the computations performed by the circuits.

The mGRASP synapse labeling technique employed here is a new methodology and we have therefore expended a substantial amount of effort to determine whether any experimental artifact has biased our analysis. While the false-positive rate associated with mGRASP is very low (approximately 0.4%), there exists, as with all LM approaches, the presence of false negatives (Yook et al., 2013). Yet the presence of false negatives should not impact our present analysis as long as the rate does not substantially vary in a systematic manner from branch to branch or synapse to synapse. In support of this we found no appreciable level of branch- or synapse-specific variability in mGRASP expression in either the pre- or the postsynaptic components. Additionally we found no depth-dependent systematic variation in synapse number through z stack imaging. Thus, the control data presented here as well as in two previous reports (Feng et al., 2012; Kim et al., 2012) lend credence to our interpretation that a high degree of spatial structure exists in the synaptic connections between CA3 and CA1 pyramidal neurons.

The structured connectivity patterns we report here have been suggested to underlie synaptic activity patterns and postsynaptic membrane potential signals observed in vivo (Lavzin et al., 2012; Lee et al., 2012; Makino and Malinow, 2011; McBride et al., 2008; Smith et al., 2013; Takahashi et al., 2012). While more work is needed to determine whether temporally matched neurons in the hippocampus also share common feature selectivity such a feature selectivity bias has already been observed within the visual cortex (Li et al., 2012). It will also be important to further explore the hypothesis that migration timing and gene expression patterns produce preferential targeting of synapse formation that could be subsequently enhanced through synaptic and dendritic plasticity (Thompson et al., 2008). These

mechanisms could produce structured connectivity patterns that would fully engage the active properties of neuronal dendrites, allowing neurons to operate as spatiotemporal input pattern detectors, thus enhancing the ability of the postsynaptic neurons to extract features embedded within their input. While this enhanced sensitivity to the particular combinations of inputs that compose biased branches may seem to reduce the flexibility of the network computation, such biases are likely to be dynamically shaped over time and even with strong structural biases the total number of patterns that a network can potentially respond to remains astronomical. Therefore, neuronal circuits could use biased connectivity patterns to enhance their ability to extract information while maintaining a full representational richness. Moreover, the presence of partially preconfigured neuronal ensembles might underlie some aspects of hippocampal network dynamics (Dragoi and Tonegawa, 2013; McNaughton et al., 2006).

EXPERIMENTAL PROCEDURES

mGRASP Labeling and Detection

(1) For broad presynaptic labeling, as previously described (Kim et al., 2012), Cre-independent pre-mGRASP (aavCAG-pre-mGRASP-mCerulean, available in Addgene) and Cre-dependent “switch on” post-mGRASP AAV (aavCAG-Jx-rev-post-mGRASP-2A-dTomato, available in Addgene) ($\sim 2 \times 10^{12}$ pfu/ml) were injected into left CA3 and right CA1 (P60~75), respectively, after in utero electroporation of paavCAG-iCre (2 $\mu\text{g}/\mu\text{l}$) into hippocampal CA1 progenitor cells in the right lateral ventricle (E15.5). To obtain clearly separate expression of pre- and postsynaptic mGRASP components we used the commissural projections from CA3 to CA1 that have been shown to roughly follow the same topographic organization and functional connectivity of ipsilateral projections (Finnerty and Jefferys, 1993). (2) To label specific temporally matched subpopulations, CA3 and CA1 progenitor cells of both ventricles were both transduced with rAAV expressing Cre recombinase (aavCAG-iCre, $\sim 2 \times 10^{12}$ pfu/ml) in utero (E15.5). Both Cre-dependent “switch-on” pre- (aavCAG-Jx-rev-pre-mGRASP-mCerulean) and post-mGRASP AAV (aavCAG-Jx-rev-post-mGRASP-2A-dTomato) were stereotaxically injected into left CA3 and right CA1 (P60~75), respectively. Stereotaxic coordinates of CA1 were anteroposterior (AP) -2.0 mm relative to bregma, mediolateral

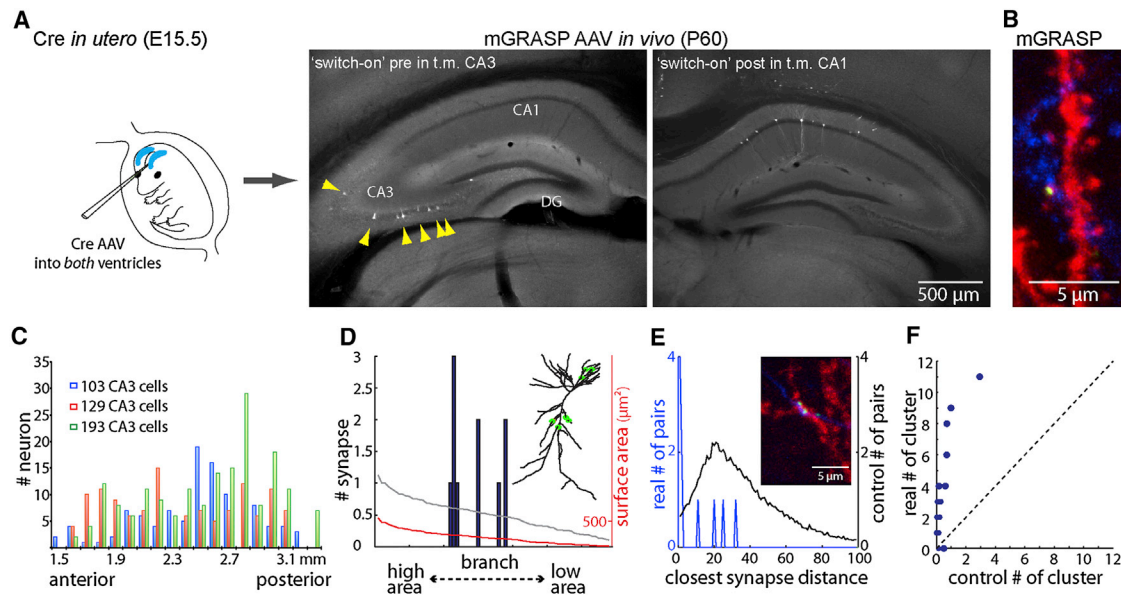


Figure 8. Enhanced Structure of Synaptic Connectivity between Temporally Matched CA3-CA1 Connection

(A) Labeling of temporally matched (t.m.) subpopulations of CA3-CA1 neurons: rAAV expressing Cre recombinase was *in utero* injected into CA3 and CA1 progenitor cells of both ventricles on E15.5. Both Cre-dependent “switch on” pre- and post-mGRASP were injected into left CA3 and right CA1, respectively, on postnatal day 60~75. Example fluorescent images show sparse CA3 temporally matched neurons expressing pre-mGRASP indicated by yellow arrowheads (left) and sparse CA1 temporally matched neurons expressing post-mGRASP (right).

(B) Example dendrite showing sparse reconstituted mGRASP signals in temporally matched CA3-CA1 connection.

(C) Bar graph represents spatial distribution of temporally matched presynaptic CA3 cells from three animals, each plotted with a different color.

(D) Bar plot of synapse number per branch; overlaid red line indicates the surface area of each branch (right y axis) and expected number of synapses in control Poisson distribution (left y axis); gray line indicates 1 SD of expected synapse number. Synapse locations on a neuTube-traced CA1 cell are shown in inset.

(E) Distribution of intersynapse distances for measured results (blue) shows more clusters than the expected distribution in random control model (green). Inset shows example dendrites exhibiting multiple synaptic contacts detected by mGRASP signals (green) in temporally matched CA3 (blue)-CA1 (red) connection.

(F) Scatter plot of the expected number of clusters in control model against the actual measured number of clusters shows notably more synaptic clusters between temporally matched subpopulations of CA3-CA1 neurons than in the broad CA3-CA1 condition as well as control model. Each dot represents a neuron. See also [Movie S5](#).

(ML) +1.6 mm and ventral (V) 1.05–1.15 mm and those of CA3 were AP –2.06 mm, ML –2.4 and –2.625 mm, and V 1.95–2.15 mm ventral. We injected 40–50 nl of viral suspension (titer, $2\sim7 \times 10^{12}$ pfu/ml). All animal procedures were conducted in accordance with protocols approved by the Institutional Animal Care and Use Committee (IACUC) at the Janelia Farm Research Campus, HHMI, and the Korea Institute of Science and Technology. Brain slices were prepared and imaged with LSM 780, 710 microscopes (Zeiss), as previously described (Kim et al., 2012). Synaptic contacts were detected using the advanced neuTube and Matlab (MathWorks)-based mGRASP detection software (Feng et al., 2012; Kim et al., 2012).

Immunostaining and Quantification

Brains were fixed and sliced on P50~60 after *in utero* electroporation (E15.5) of paavCAG-post-mGRASP-2A-dTomato (2 $\mu\text{g}/\mu\text{l}$). Fixed 50 μm slices were permeabilized with 0.4% Triton-X in Tris-buffered saline (TBS) for 30 min at room temperature (RT). After preblocking with TBS containing 5% normal goat serum (NGS) and 0.4% Triton-X for 30 min at RT, slices were incubated with antibodies in TBS containing 2% NGS and 0.4% Triton-X overnight at 4°C and followed by incubation with Alexa-conjugated secondary antibodies for 2 hr at RT. dTomato signals were amplified by sequential staining. Antibodies were as follows: anti-GFP (Invitrogen, 1:1,000 and abcam, 1:500), anti-DsRed (Clontech, 1:200), and Alexa 488, 555, 647-conjugated secondary antibodies (Invitrogen, 1:300~500). The post-mGRASP distribution was analyzed on three different levels: branch, segment, and spine. In the branch level, the correlation between the number of branch voxels and the number of post-mGRASP-positive voxels was calculated. In the segment level, average intensity of post-mGRASP signals of each segment was shown as co-

lor maps. In the spine level, spines and post-mGRASP components of branches from the top of slice were manually marked; approximately 97% of spines were post-mGRASP positive.

Synapse Data Analysis

Reconstructed branches in neuTube were approximated as a series of joined small tubes with fixed radii, allowing the length and surface area of each branch to be estimated. For each neuron we calculated the total surface area and the total number of synaptic contacts; dividing the number of contacts by the area gave the average density of synaptic contacts. All data analysis was performed in custom software written in Matlab. Sections below describe specific analyses.

1. Subclassification of Branches

The classic definition of a pyramidal cell divides the branches into two categories, apical dendrites and basal dendrites, which are located on opposite sides of the soma. For more detailed analysis, we further categorized the branches into the following subclasses. Main trunk: any apical thickest branch connecting tuft branches and the soma. Apical tuft branch: any distal apical branch in stratum lacunosum-moleculare bifurcating from the main trunk. Apical/basal terminal branch: other than apical tuft branch, any apical/basal branch terminated without connecting to anything else. Apical/basal intermediate branch: other than main trunks, any apical/basal branch connecting to the soma or another branch at both ends.

2. Branch-Level Analysis

For each neuron we calculated the total surface area of the relevant dendritic arbor and the total number of synaptic contacts. Dividing the number of contacts by the area gave the average density of synaptic contacts, the one free

parameter of the Poisson distribution. The expected synapse number and its variability for each branch are given by this distribution, and deviations from synapse number were analyzed. To determine the statistical significance of these deviations, all branches were pooled together and the Benjamini and Hochberg step-up procedure (Benjamini and Hochberg, 1995) was used to correct for multiple comparisons. Branches found significantly different from chance were then traced back to their neuron of origin, and the fraction of branches significantly different from chance was calculated. R^2 values were calculated for the linear regression of synapse number from branch surface area. The summary statistic reporting the selectivity of each neuron was the maximal difference from the mean, normalized by standard deviation (Z score). We repeated all analyses with dendritic branch length instead of branch area and found no qualitative difference in the results.

3. Peters's Rule Analysis

To directly determine the accuracy of Peters's rule analysis we tested for a linear correlation between synaptic density and the product of dendritic branch area and presynaptic axonal density on a cell-by-cell basis and with all data aggregated together. A matching control model for each neuron was generated by drawing the synapse number independently for each branch from a Poisson distribution with a rate proportional to the Peters's rule value for each branch (i.e., the product of average branch axonal density and branch number). In presenting the aggregate data (Figure 3B) we normalized the synapse number to the average synaptic density for this neuron to control for variability in synaptic density among different neurons. To address the issue of nonuniformities of axonal density over scales smaller than that of the average branch we repeated the analyses above while breaking each branch into smaller units (values of 15, 30, 50 μm were used). No qualitative differences were found in this "broken branch" analysis.

To further analyze Peters's rule on the population level we divided branches into three groups: those showing no significant deviations from chance; those with significantly greater synaptic density; and those with significantly lower synaptic density. To determine the available presynaptic axonal density we measured mCerulean-tagged pre-mGRASP by finding the intensity of the blue channel; this signal corresponds to axonal labeling in an extended cylinder surrounding each segment of dendrite (radius of the traced tube plus $\sim 2.5 \mu\text{m}$). We then averaged the available presynaptic axonal density value separately in each one of the three branch groups. To determine how accurately the available presynaptic axonal density can be used to predict whether the density of synaptic contacts will be greater or lesser than chance we performed a receiver operating characteristic (ROC) analysis. Briefly, in ROC analysis one changes continuously the value of a predictor from its lowest possible value to its highest possible value and records the fraction (or percentage) of true positives and false positives for the different predictor values. At the lowest predictor value there are no positives at all and therefore no true or false positives. At the highest predictor value, every example is considered positive and therefore the fraction of both true and false positives is 1. The ROC curve visualizes the tradeoffs between true and false positives. To test Peters's rule on the single neuron level we related the deviation in number of synapses to the available presynaptic density and compared the experimental data to a simple model where synaptic locations were randomly generated according to Peters's rule, i.e., the number of synapses was proportional to the product of dendritic surface area and available presynaptic density. We repeated all analyses with dendritic branch length instead of branch area and found no qualitative difference in the results.

4. Clustering Analysis

To analyze whether synapses on a branch were clustered or distributed randomly we performed two types of analysis. First, on a branch-by-branch level, we examined the distances between pairs of (spatially consecutive) synapses. If the synapses were distributed randomly, the distances between the synapses should follow an exponential distribution. We compared the actual distribution per branch to an exponential distribution via the Lilliefors test (Lilliefors, 1969). Having corrected for multiple comparisons we determined which branches significantly deviated from this distribution and reported for each neuron the fraction of the branches that were identified as significantly clustered. The deviations from the exponential distribution we observed, mainly an overabundance of short inter-synapse intervals, are consistent with clustering. Therefore, we define a cluster as a pair of

synapses with a given intersynapse-distance (1.5 μm) between them (or lower).

This type of analysis can be performed on a single branch or by aggregating branches that have similar synaptic densities. However, since branch synaptic density varied considerably within a single neuron it cannot be applied to the neuron as a whole. To analyze synaptic clustering on the neuron level (and in a way complimentary to the previously described analysis) we calculated the distances between each synapse and its nearest neighbor in space, following a branch path. We then compare this distribution of nearest neighbor distances to a randomized synapse location according to the control Poisson distribution. For the data set of temporally matched neurons we didn't identify enough synapses to be able to reliably compare the intersynapse intervals on a single branch to the exponential distribution; we therefore used only the whole neuron analysis.

A cluster can result from either multiple, different axons creating synapses in close proximity, or from multiple synapses formed by the same, single axon. To look more closely at this issue, we estimated the probability of single axons creating multiple synaptic contacts. Specifically, we first estimated the number of relevant axons in the presynaptic population by measuring the number of synapses and dividing that number by the average number of synapses created by a single axon. We derived this number from a published account of the average numbers of multiple synaptic contacts (Sorra and Harris, 1993: 76% single contact, 4% multiple contacts on the same branch, 17% two contacts on two branches, 2% three contacts on three branches, 1% four contacts on four branches). To ensure we do not underestimate the number of clusters created by single axons, we make the assumption that all multiple contacts created on the same branch would occur at mutual distances that we would count as a cluster by all our criteria. Accordingly, we estimate the number of single-axon clusters expected by the 4% of multiple contacts upon a single branch times the estimated number of axons.

SUPPLEMENTAL INFORMATION

Supplemental Information includes four figures and five movies and can be found with this article online at <http://dx.doi.org/10.1016/j.neuron.2013.11.026>.

AUTHOR CONTRIBUTIONS

J.C.M. and J.K. conceived the project and designed the experiments. C.Y., B.L., and J.K. performed molecular biology, animal surgery, immunostaining, and imaging. L.F. and T.Z. developed stitching, tracing, and detection programs. S.D. designed and performed all statistical data analysis. S.D., J.C.M., and J.K. wrote the paper.

ACKNOWLEDGMENTS

We thank Attila Losonczy for many valuable discussions; Mark Harnett and Aaron Milstein for comments on the manuscript; and Miran Son for technical support. This work was supported by the KIST Institutional Program (Project No. 2E24210) and the World Class Institute Program of the National Research Foundation of Korea (L.F., C.Y. B.L. and J.K.).

Accepted: November 6, 2013

Published: January 9, 2014

REFERENCES

- Bannister, N.J., and Larkman, A.U. (1995). Dendritic morphology of CA1 pyramidal neurones from the rat hippocampus: II. Spine distributions. *J. Comp. Neurol.* 360, 161–171.
- Benjamini, Y., and Hochberg, Y. (1995). Controlling the false discovery rate: a practical and powerful approach to multiple testing. *Journal of the Royal Statistical Society (Methodological)* 57, 289–300.
- Branco, T., Clark, B.A., and Häusser, M. (2010). Dendritic discrimination of temporal input sequences in cortical neurons. *Science* 329, 1671–1675.

- Brown, S.P., and Hestrin, S. (2009). Intracortical circuits of pyramidal neurons reflect their long-range axonal targets. *Nature* 457, 1133–1136.
- Deguchi, Y., Donato, F., Galimberti, I., Cabuy, E., and Caroni, P. (2011). Temporally matched subpopulations of selectively interconnected principal neurons in the hippocampus. *Nat. Neurosci.* 14, 495–504.
- Dragoi, G., and Tonegawa, S. (2013). Distinct preplay of multiple novel spatial experiences in the rat. *Proc. Natl. Acad. Sci. USA* 110, 9100–9105.
- Feng, L., Zhao, T., and Kim, J. (2012). Improved synapse detection for mGRASP-assisted brain connectivity mapping. *Bioinformatics* 28, i25–i31.
- Finnerty, G.T., and Jefferys, J.G. (1993). Functional connectivity from CA3 to the ipsilateral and contralateral CA1 in the rat dorsal hippocampus. *Neuroscience* 56, 101–108.
- Gasparini, S., and Magee, J.C. (2006). State-dependent dendritic computation in hippocampal CA1 pyramidal neurons. *J. Neurosci.* 26, 2088–2100.
- Harvey, C.D., and Svoboda, K. (2007). Locally dynamic synaptic learning rules in pyramidal neuron dendrites. *Nature* 450, 1195–1200.
- Ishizuka, N., Weber, J., and Amaral, D.G. (1990). Organization of intrahippocampal projections originating from CA3 pyramidal cells in the rat. *J. Comp. Neurol.* 295, 580–623.
- Jia, H., Rochefort, N.L., Chen, X., and Konnerth, A. (2010). Dendritic organization of sensory input to cortical neurons in vivo. *Nature* 464, 1307–1312.
- Kim, J., Zhao, T., Petralia, R.S., Yu, Y., Peng, H., Myers, E., and Magee, J.C. (2012). mGRASP enables mapping mammalian synaptic connectivity with light microscopy. *Nat. Methods* 9, 96–102.
- Kleindienst, T., Winnubst, J., Roth-Alpermann, C., Bonhoeffer, T., and Lohmann, C. (2011). Activity-dependent clustering of functional synaptic inputs on developing hippocampal dendrites. *Neuron* 72, 1012–1024.
- Krueppel, R., Remy, S., and Beck, H. (2011). Dendritic integration in hippocampal dentate granule cells. *Neuron* 71, 512–528.
- Lavzin, M., Rapoport, S., Polsky, A., Garion, L., and Schiller, J. (2012). Nonlinear dendritic processing determines angular tuning of barrel cortex neurons in vivo. *Nature* 490, 397–401.
- Lee, D., Lin, B.J., and Lee, A.K. (2012). Hippocampal place fields emerge upon single-cell manipulation of excitability during behavior. *Science* 337, 849–853.
- Legenstein, R., and Maass, W. (2011). Branch-specific plasticity enables self-organization of nonlinear computation in single neurons. *J. Neurosci.* 31, 10787–10802.
- Li, X.G., Somogyi, P., Ylinen, A., and Buzsáki, G. (1994). The hippocampal CA3 network: an in vivo intracellular labeling study. *J. Comp. Neurol.* 339, 181–208.
- Li, Y., Lu, H., Cheng, P.L., Ge, S., Xu, H., Shi, S.H., and Dan, Y. (2012). Clonally related visual cortical neurons show similar stimulus feature selectivity. *Nature* 486, 118–121.
- Lilliefors, H.W. (1969). On the Kolmogorov-Smirnov Test for the Exponential Distribution with Mean Unknown. *J. Am. Stat. Assoc.* 64, 387–389.
- Losonczy, A., and Magee, J.C. (2006). Integrative properties of radial oblique dendrites in hippocampal CA1 pyramidal neurons. *Neuron* 50, 291–307.
- Losonczy, A., Makara, J.K., and Magee, J.C. (2008). Compartmentalized dendritic plasticity and input feature storage in neurons. *Nature* 452, 436–441.
- Makino, H., and Malinow, R. (2011). Compartmentalized versus global synaptic plasticity on dendrites controlled by experience. *Neuron* 72, 1001–1011.
- McBride, T.J., Rodriguez-Contreras, A., Trinh, A., Bailey, R., and DeBello, W.M. (2008). Learning drives differential clustering of axodendritic contacts in the barn owl auditory system. *J. Neurosci.* 28, 6960–6973.
- McNaughton, B.L., Battaglia, F.P., Jensen, O., Moser, E.I., and Moser, M.B. (2006). Path integration and the neural basis of the 'cognitive map'. *Nat. Rev. Neurosci.* 7, 663–678.
- Megias, M., Emri, Z., Freund, T.F., and Gulyás, A.I. (2001). Total number and distribution of inhibitory and excitatory synapses on hippocampal CA1 pyramidal cells. *Neuroscience* 102, 527–540.
- Mishchenko, Y., Hu, T., Spacek, J., Mendenhall, J., Harris, K.M., and Chklovskii, D.B. (2010). Ultrastructural analysis of hippocampal neuropil from the connectomics perspective. *Neuron* 67, 1009–1020.
- Nicholson, D.A., Trana, R., Katz, Y., Kath, W.L., Spruston, N., and Geinisman, Y. (2006). Distance-dependent differences in synapse number and AMPA receptor expression in hippocampal CA1 pyramidal neurons. *Neuron* 50, 431–442.
- Peters, A., and Feldman, M.L. (1976). The projection of the lateral geniculate nucleus to area 17 of the rat cerebral cortex. I. General description. *J. Neurocytol.* 5, 63–84.
- Poirazi, P., Brannon, T., and Mel, B.W. (2003). Pyramidal neuron as two-layer neural network. *Neuron* 37, 989–999.
- Polsky, A., Mel, B.W., and Schiller, J. (2004). Computational subunits in thin dendrites of pyramidal cells. *Nat. Neurosci.* 7, 621–627.
- Smith, S.L., Smith, I.T., Branco, T., and Häusser, M. (2013). Dendritic spikes enhance stimulus selectivity in cortical neurons in vivo. *Nature* 503, 115–120.
- Sorra, K.E., and Harris, K.M. (1993). Occurrence and three-dimensional structure of multiple synapses between individual radiatum axons and their target pyramidal cells in hippocampal area CA1. *J. Neurosci.* 13, 3736–3748.
- Spruston, N. (2008). Pyramidal neurons: dendritic structure and synaptic integration. *Nat. Rev. Neurosci.* 9, 206–221.
- Takahashi, N., Kitamura, K., Matsuo, N., Mayford, M., Kano, M., Matsuki, N., and Ikegaya, Y. (2012). Locally synchronized synaptic inputs. *Science* 335, 353–356.
- Thompson, C.L., Pathak, S.D., Jeromin, A., Ng, L.L., MacPherson, C.R., Mortrud, M.T., Cusick, A., Riley, Z.L., Sunkin, S.M., Bernard, A., et al. (2008). Genomic anatomy of the hippocampus. *Neuron* 60, 1010–1021.
- Ujfalussy, B.B., and Lengyel, M. (2011). Active dendrites: adaptation to spike-based communication. In *Advances in Neural Information Processing Systems*, pp. 1188–1196.
- Varga, Z., Jia, H., Sakmann, B., and Konnerth, A. (2011). Dendritic coding of multiple sensory inputs in single cortical neurons in vivo. *Proc. Natl. Acad. Sci. USA* 108, 15420–15425.
- Yook, C., Druckmann, S., and Kim, J. (2013). Mapping mammalian synaptic connectivity. *Cellular and molecular life sciences. Cell. Mol. Life Sci.* 70, 4747–4757.
- Yu, Y.C., Bultje, R.S., Wang, X., and Shi, S.H. (2009). Specific synapses develop preferentially among sister excitatory neurons in the neocortex. *Nature* 458, 501–504.